INSTITUTE OF COMPUTER SCIENCES
Master in Artificial Intelligence and Data Science

Universitätsstr. 1 D–40225 Düsseldorf

Heinrich Heine Universität Düsseldorf

# AI-based fluorescent labeling for cell line development

**Hanna Pankova**

Master thesis

Date of issue: 01. April 2022
Date of submission: 29. August 2022
Reviewers: Prof. Dr. Markus Kollmann
Dr. Wolfgang Halter

## Erklärung

Hiermit versichere ich, dass ich diese Master thesis selbstständig verfasst habe. Ich habe dazu keine anderen als die angegebenen Quellen und Hilfsmittel verwendet.

Düsseldorf, den 29. August 2022

Hanna Pankova

## Abstract

Cell line development is an expensive and time-consuming process, however that is the most modern approach for producing the proteins needed in various pharmaceuticals.

# Contents

# 1 Introduction

## 1.1 Motivation

Nowadays recombinant proteins are widely used in biomedical research and production of medicines that are used in the variety of therapeutic neeeds like vaccines and antibodies [TODO add references]. Therefore there is currently a great need for high-volume and high-quality recombinant protein production. That is why the optimization and improvement of cell line development (CLD) as a process in use for the production of recombinant proteins is extremely important.

Clone screening is a step of the CLD process in which cells are analyzed for further selection of the most stable and productive clones. Fluorescence microscopy provides data about the cell structure that enables better clone selection, however it is not only expensive and time-consuming, but also toxic for the cells. Automating fluorescence microscopy for clone selection via convolutional neural networks *in silico* significantly simplifies the existing procedure of clone selection, reducing phototoxicity, time and expenses needed for the analysis.

The goal of this thesis is to provide a proof of concept on whether an *in silico* approach to fluorescent labeling can substitute manual cell staining and provide all the needed information that would be used for further clone screening and selection. That is particularly why the research at hand is aimed towards the specific needs, pipelines and data used at Merck KgaA. In this research four UNet models (for four target proteins highlighting different cell organelles) were developed for automating fluorescence cell staining based on DIC microscopy imaging of CHO cells: nuclei, endoplasmic reticulum, [[green fluorescent protein]] and Golgi apparatus. Another important goal of this research that differentiates it from the similar studies like [TODO cite LaChance 2020 and cite Christiansen 2018] is to not only provide deep learning models for the fluorescence predictions but also study their reliability and be able to detect drift during image acquisition that can happen quite easily due to the sensitivity of the microscope settings as well as the cell phenotypes, scaling and fixation procedures.

This thesis is laid out as follows: Section 2 reviews the biological concepts needed to understand the application of this research, it also reviews machine and deep learning concepts used for data analysis; Section 3 provides an overview of the implementation and the results of the experimental *in silico* fluorescence predictions; Section 4 shows stability of the deep learning models developed in the previous section and provides valuable insights on the information from their embeddings; Section 5 details the practical tools used for the development at Merck KgaA and Section 6 explores possible future research questions that arose from the current analysis and provides concluding remarks and succinct recommendations.

## 1.2 Notation

$\boldsymbol{x}^{(i)}$ The i-th input image (sample) from a dataset

$\boldsymbol{X}_{train}$ A set of training examples

$\boldsymbol{y}^{(i)}$ The target image associated with the i-th input sample from a dataset

$p_{data}$ Data generating distribution

# 2 Domain knowledge

The *in silico* fluorescence labeling approach has proven to be very promising as a substitute to the manual cell staining processes [TODO cite all the relevant references]. For example, the research of [TODO cite Christiansen 2018] did not only prove successful prediction of different cell stains with a variety of modalities and cell types, but it had also successfully determined cell viability. Nevertheless, the study is limited mainly to transmitted light (TL) z-stack imaging. This refers to the networks input being comprised of 3D images, which is not the case in this work. [cite Ounkomol 2018] too shows succeful predictions of several organelles in bright-field TL 3D images using 3D convolutional neural networks. However, switching to 2D data did not yield adequate results for them. Other, newer studies like [cite Ugawa 2021] provide an application of label-free fluorescence predicting already at the sorting stage, when a high-throughput system sorts cells individually. However, only a single-pixel detector is used by this study, meaning that it captures a wave rather than an image. Nonetheless one can recover an image with heavy computations if needed [cite Sadao Ota 2018].

There are two very promising studies by [cite Cheng 2021] and [cite LaChance 2020]. Even though the former manages to reach a state-of-the art performance on label-free fluorescence reconstruction, it uses reflectance images from oblique dark-field illumination as the input, which is a more specific cell imaging approach. Still, this input provides higher structural contrast in comparison to any transmission technique [cite Boustany 2010]. The latter study uses an easier imaging technique (DIC imaging) as an input, which shows great results even with low-resolution data. Both of these studies provide results based not only on training metrics, but also on performance of the models for metrics used in the downstream tasks. This is very important in the label-free fluorescence labeling research and was not present in papers before LaChance. In the thesis at hand, many methods from the LaChance paper were used as both the data and the processes in the project pipeline of Merck KgaA align very well with the study conducted in that paper.

All of the studies mentioned above, as well as this work rely on the premise that the input imaging type (here DIC) contains enough information to predict the fluorescence signal from it. This is a reasonable assumption because DIC, as well as bright-field and phase contrast imaging, are very often used for determining cell morphology [TODO cite Kasprowicz 2017].

This chapter provides a brief overview of the biological background needed to understand the process of cell line development (CLD) and the role of fluorescent *in silico* labeling of DIC cell images within. It also covers the fundamentals of deep and machine learning techniques used here including clustering and dimensionality reduction approaches. At the end of the chapter, a brief summary of the microscopy image acquisition process used in the research is given.

## 2.1 Biology

### 2.1.1 Cell line development process

#### 2.1.1.1 Cell line development with CHO cells

Cell line development (CLD) is a process of generating single cell-derived clones that produce high and consistent levels of target therapeutic protein [TODO cite pharma.lonza.com/offerings/mammalian/cell-line-development]. Therapeutic proteins in this case are so-called recombinant proteins and they are spreadly used in the biomedical research, medicine production and for many different therapeutic needs like, for example, vaccines or monoclonal antibodies (mAbs) [TODO cite Ohtake 2013, Jefferis 2021, Funaro 1996]. A recombinant protein is defined by [cite Barbeau, J] as a modified or manipulated protein encoded by a recombinant DNA. Recombinant DNA in its turn consists of a plasmid, where the genes of a target protein of interest are cloned downstream of a promoter region. As soon as this plasmid will be transfected to a host cell (for example some mammalian cells that are able to produce the protein), the host wil start to express of this protein of interest. In nowadays industry and research there is a great need for production of recombinant proteins in high volumetric amounts and of a good quality [TODO cite Tihanyi 2020]. That is why the goal on many researches is in recombinant protein production is to create a their efficient expression and high-throughput systems to improve the CLD processes [cite Tihanyi 2020].

One of the most popular host cells used in CLD and in this work specifically are chinese hamster ovary (CHO) cells [cite Castan 2018]. Altough different cells can be used as hosts like bacterial, plant-based, yeast cells, the most popular ones remain mammalian [cite Beckman]. The reason behind this popularity hides in the fact that they can produce diverse correctly folded proteins and most importantly they have high productivity protein production rates. Productivity rate is measured in titre of produced protein, and CHO cells can reach 0.1 - 1 g/L in batch and 1-10 g/L in fed-batch cultures [cite Tihanyi 2020]. Mostly all of the mAbs are produced using CHO cells [cite Lalonde 2017]. Companies mostly use the same host cell line for their productions because already checked and qualified cells simplify the road to the clinic [cite Tihanyi 2020]. That is why current research has a wide applicability.

However there is a downside in using CHO as host cells - they are well-known by their instability. As a rapidly growing immortal cells CHO also genomically unstable and extremely heterogeous which ususally leads to their main problem - production instability. The problem of choosing the stable and high producing clones that simutaneously will be able to express protein quailitatively and quantitably over time is essentially the main goal of nowadays research. The big challenge in manufacturing here are the time and costs of production. Currently a lot of research attention is dedicated to the reduction of both as well as to developing techniques of high-throughput clone screening and characterization [cite Tihanyi 2020]. The latter one is of interest for this thesis. With the great amounts of data acquired over time and the development of the computational modelling and statistical analysis it is possible now to do the analysis *in silico*, meaning - computationally without intervening into the cells instead of the usual *in vitro* analysis.

#### 2.1.1.2 CLD steps

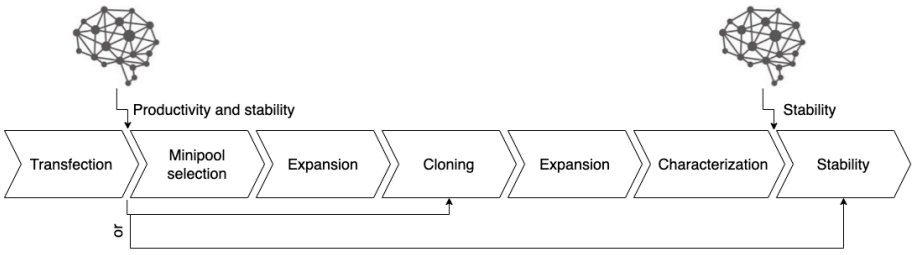


Figure 1: CLD process steps

First step of CLD is called transfection - the introduction of the gene of interest (GOI or a DNA vector or alternatively an expression vector) to CHO cells. And it has two main problems: first is that the transfection mostly results in a vector being inserted into a random site within a host cell genome and second, that it generally has low efficiency of integration [cite Tihanyi]. It is important to transfect a GOI into an optimal site of genome to secure a high protein expression over time during protein production, however pratically transfection happens into a random location of genome. In cases when the gene was transfected into the inactive site of genome (and essentially the majority of genome is transriptionally inactive) the cell will likely not be able to express the gene [cite Castan, Hong 2018].

The second step of the process is selection of cells minipools that have successful and stable gene integrations for further expansion and cloning. The reason why not all of them are suitable is the following: during the transfection step only 80% of the cells will recieve a vector of GOI [cite Castan]. Only a small percent of these cells actually integrate a vector into the genome and, as mentioned above, only a fraction of those are able to stabily express the protein. [a better reference needed Shin 2020]. After the best mini pools are selected, they will be expanded.

The third step in CLD is to clone the cells. Chosen stable pools of cells are phenotypically and genetically diverse - meaning they have different growth rates, metabolic profile and etc. This is not ideal for industrial production - all the cells used for protein production should be derived from the same clone [cite [25] from Castan].

Once the cells are cloned, phenotypical and genetical heterogeneity is reduced, the next step is to charaterize the cells for their expression of the GOI. One has to estimate clones productivity and stability. Such observations may take up to 90 days (usually the checks are made on the day 30, day 60 and day 90). If the clones remain stable after this time and are able to express enough of the protein, then they are suitable for further production. However this last step consumes a lot of time and maintaining costs for feeding and analysing the cells.Predicting productivity and stability of the cells on ealier stages would reduce this time significantly or even allow to escape this process completely.

### 2.1.2 Project specifications of cell line development for Merck KgaA

There are many different proteins that can be produced using such technologies, for example, vaccines, hormones, sugars and etc., however this research is dedicated to the production of monoclonal antibodies (mAbs).

CHOZN® Platform is a currently widely used product of Merk KgaA. CHOZN is a CHO mammalian cell expression system for the fast and easy selection and scale up of clones producing high levels of recombinant proteins [cite tech-bulletin]. The processes of developing the expression systems on this platform correspond to the general CLD process described in the previous subsection [put subsection number]. The scope of the project is to simplify labour intensive and time-consuming process of stability determination of the expression system by inducing predictions of productivity and stability rates on early steps on the CLD process.

After the transfection step there are several quantities that are measured in minipools in order to select the best ones. For example, cell size, its complexity, cell surface protein expression, Endoplasmic Reticulum (ER)mass, Mitochondria mass and etc. For qualitative or quantitative characterization of cells fluorescent labeling is used. It is the process of covalently binding fluorescent dyes to biomolecules such as nucleic acids or proteins so that they can be visualized by fluorescence imaging [cite https://www.nature.com/subjects/fluorescent-labelling]. A fluorophore is a chemical compound that can reemit light at a certain wavelength.These compounds are a critical tool in biology because they allow experimentalists to image particular components of a given cell in detail [cite O'reilly life sciences p113].

Unfortunately fluorescence labeling is expensive, time-consuming and may ruin the cell due to its phototoxicity [cite Fried et al., 1982; Patil et al., 2018; Progatzky et al., 2013)]. Additionally, Yeo et al. [cite Tihanyi] found out that different selection markers affect the production stability of CHO cells. Other negative aspects of manual staining appoach are the following: there is a limited number of available fluorescent channels in microscopes; some fluorophores have a spectral overlap, therefore there is a limited amout of detectable markers [cite Perfetto et al., 2004]; such labels can be inconsistent [cite Burry, 2011; Weigert et al., 1970), depend a lot on reagent quality and require many hours of lab work. Toxicity for instance is a very dangerous disadvantage especially for the medince production as it may affect event the final product. Therefore there exists a need for an approach of *in silico* flurescent labeling - computationally and without intervening into the cell.

For the *in silico* labeling the inputs data is a differential interference contrast (DIC) microscopy, this is an optical microscopy technique used to enhance the contrast in unstained, transparent samples [cite wikipedia?]. This is a much cheaper image acquision technique that the staining process, and there is much less variability within it as well (no dependance on the dye or antibody quality for ex.). The research is dedicated towards predicting fluorescence signal from the DIC imaging directly without the need of cell staining. The measurements needed for selection of minipools cant hen be calculated as usual, but using the predicted images instead.

## 2.2 Deep learning and machine learning basics

Introduction of the notaiton for the dataset, parameters, predictions.

### 2.2.1 Neural networks

Convolutional neural network, Autoencoder, embedding, optimizers, regularization, descriptions of how each layer works.

Convolutional neural networks (CNNs) capture nonlinear rela- tionships over large areas of images, resulting in vastly improved performance for image recognition tasks as compared to classical machine learning methods

TODO cite Oukomol

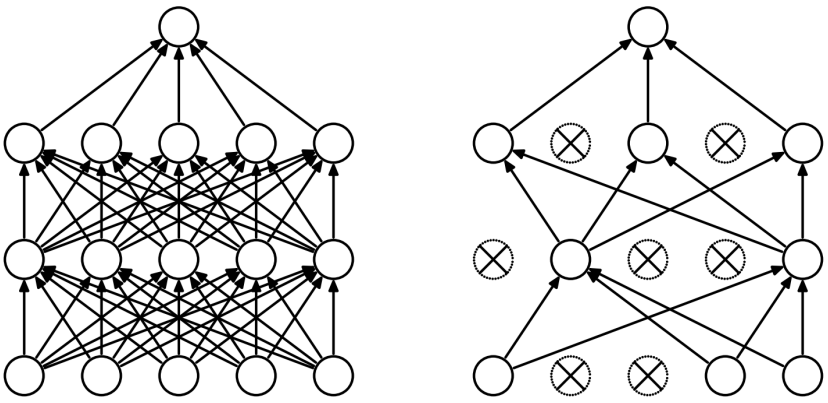

(a) Standard Neural Net (b) After applying dropout.

Figure 2: Dropout

### 2.2.2 Dimensionality reduction methods

#### 2.2.2.1 UMAP

#### 2.2.2.2 PCA

#### 2.2.2.3 PacMAP

### 2.2.3 Clustering methods

#### 2.2.3.1 DBSCAN

#### 2.2.3.2 HDBSCAN

#### 2.2.3.3 K-means

## 2.3 Imaging

### 2.3.1 Digital imaging

How image is stored in memory, which conventions there are (RGB, BGR (conventions are used in corruptions augmentations)).

### 2.3.2 Microscopy imaging

#### 2.3.2.1 Image acquisition peculiarity

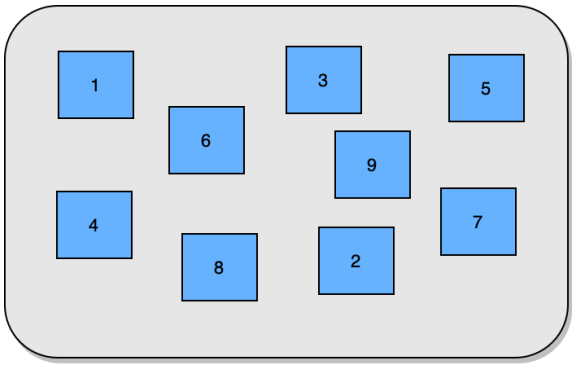


Figure 3: Way in which photos of the well-plate were taken

Which difficulties it may cause (validation loss is lower than train loss)

#### 2.3.2.2 Crops combination technique

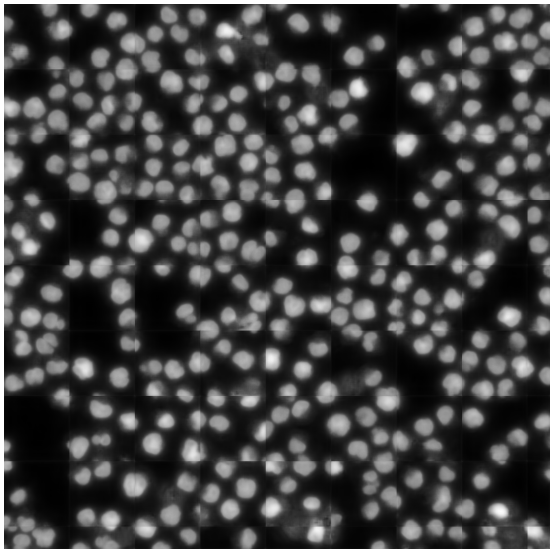

Figure 4: No overlap

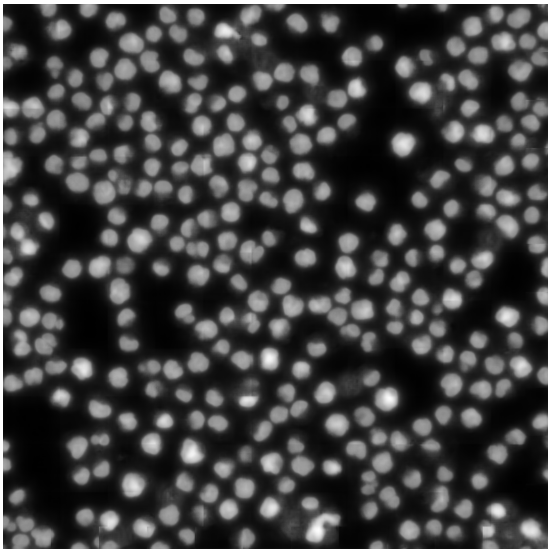

Figure 5: 30 pixels overlap

Improve this plot by showing the visible border explicitly, example of how it can influence a further segmentation perhaps?

# 3 Implementation and experiments

## 3.1 Model training

### 3.1.1 Neural network architecture

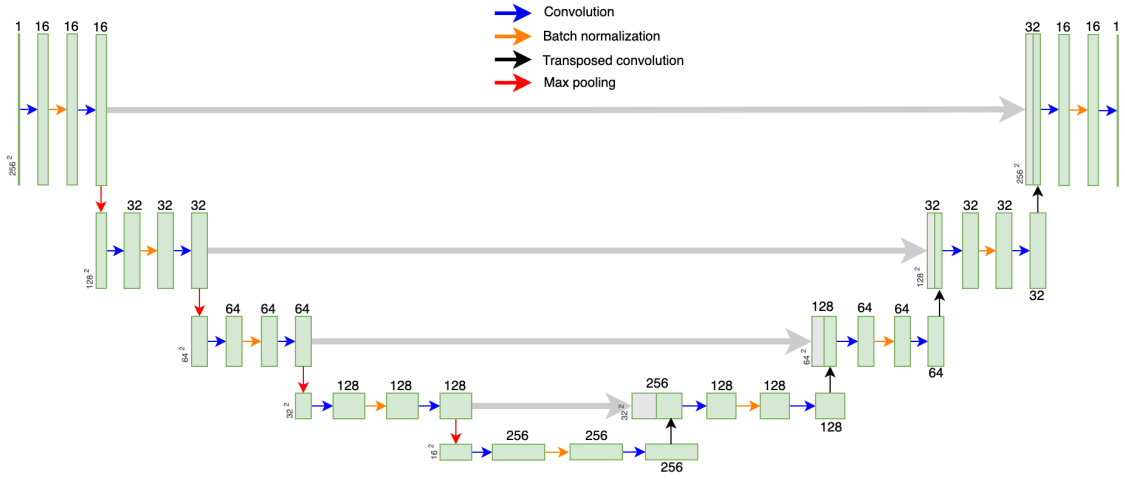


Figure 6: Unet

And information on the embeddings, output sizes, amount of parameters, etc.
take description from here file:///Users/anniepank/Downloads/media-1.pdf

### 3.1.2 Loss functions

Which loss functions were used, Pearson correlation coefficient explained.

### 3.1.3 Available data

Description of the datasets and the amount of images in each category.

Table 1: Available data for each fo the organelles

| | Total images | Training crops | Validation crops | Test crops |
|---|---|---|---|---|
| Nuclei | 595 | 27,264 | 3,008 | 7,616 |
| Actin | 400 | 18,432 | 2,048 | 5120 |
| Golgi | 761 | 23,036 | 2,336 | 6,347 |
| H19 | 400 | 27,264 | 3,008 | 7,61 |
| Nucleolei | ? | ? | ? | ? |

### 3.1.4 Training costs estimation

Table with the estimation of costs and times for AWS

### 3.1.5 Augmentations

Description of all augmentations used

#### 3.1.5.1 Special augmentations for rotation and scaling

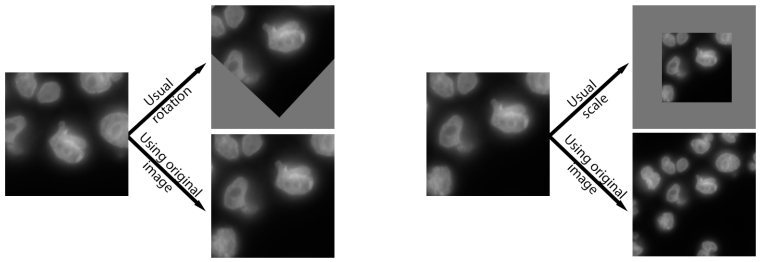


Figure 7: Using original image for rotation and scaling augmentations

### 3.1.6 Model setup

#### 3.1.6.1 Weight Initialization

These plots represent MSE

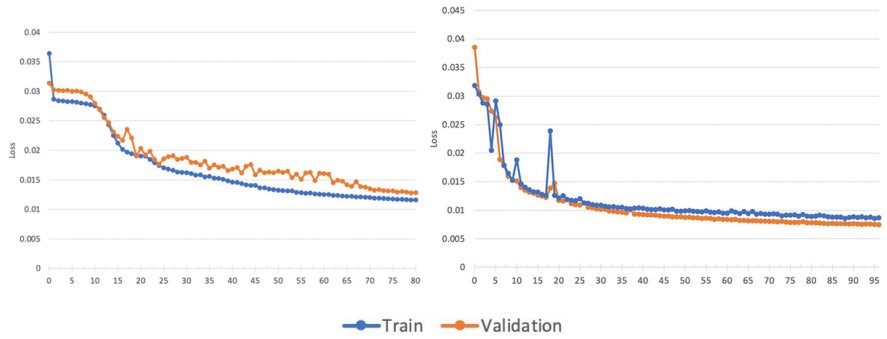


Figure 8: Nuclei training without and with custom weight initialization

#### 3.1.6.2 Regularization

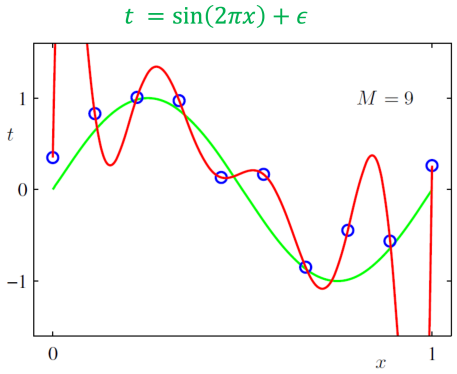


Figure 9: Overfitting

#### 3.1.6.3 Optimizers

Comparison of different optimizers

## 3.2 Nuclei

### 3.2.1 Preprocessing

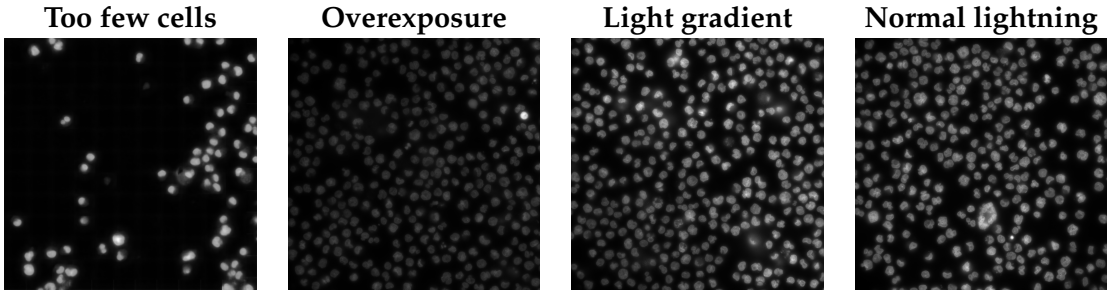


Figure 10: Different lightning conditions

#### 3.2.1.1 Thresholding algorithms

Global and local thresholding

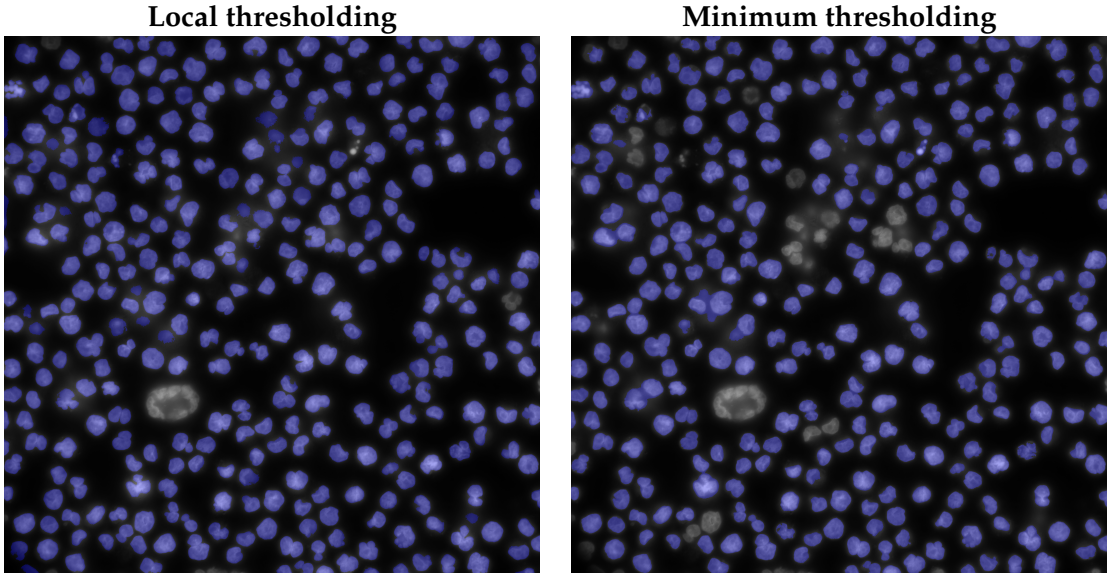


Figure 12: Local vs. Global thresholding (normal conditions)

### 3.2.2 Training and predictions

#### 3.2.2.1 Convergence

Has the model converged or not. Will more data help?

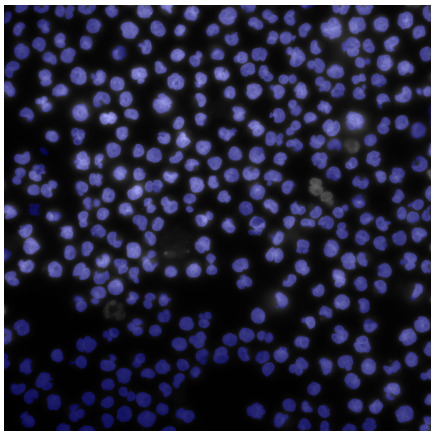

(a) Local

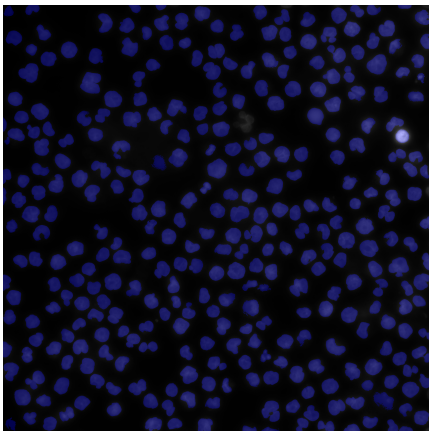

(b) Local

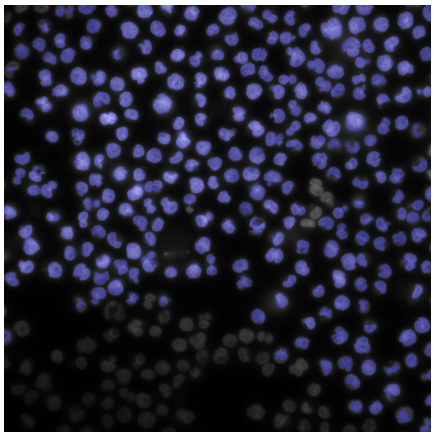

(c) Global, minimum

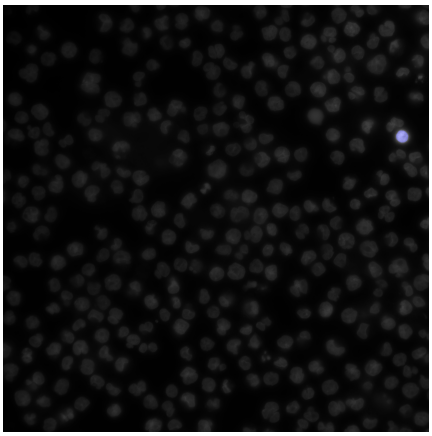

(d) Global, minimum

Figure 11: Local vs. Global thresholding

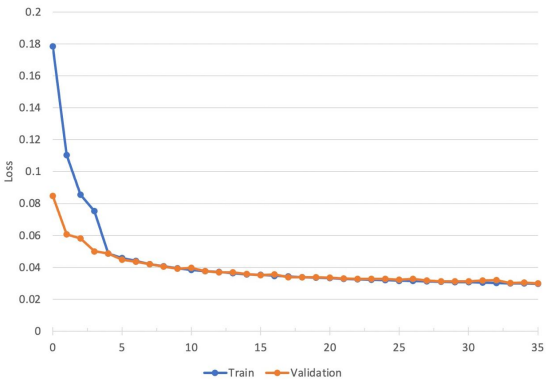


Figure 13: Having more data makes training more stable

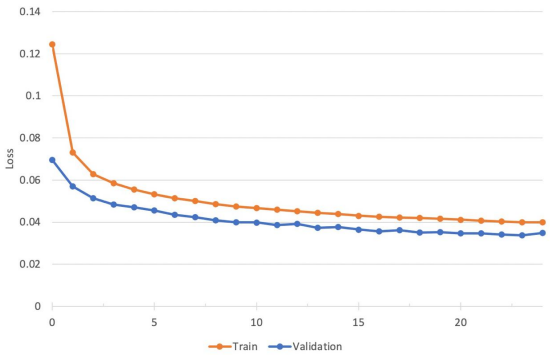


Figure 14: With regularization and augmentations PCC

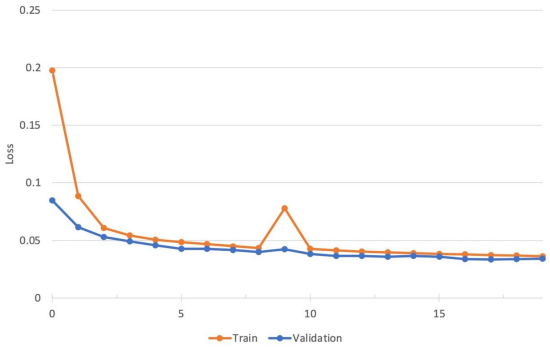


Figure 15: No regularization but augmentations

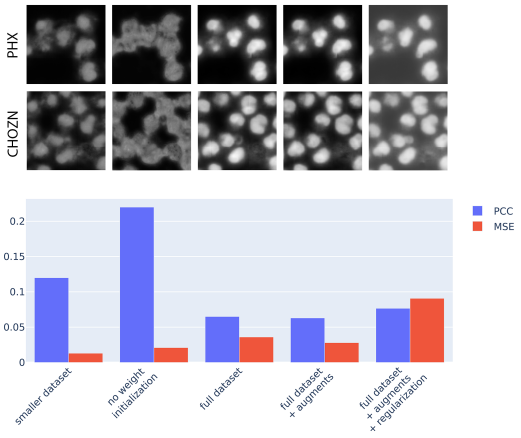


Figure 16: Difefrent models predictions and scores comparison

#### 3.2.2.2 Predictions quality

Blurry, boundaries, not enough of details and possible improvements

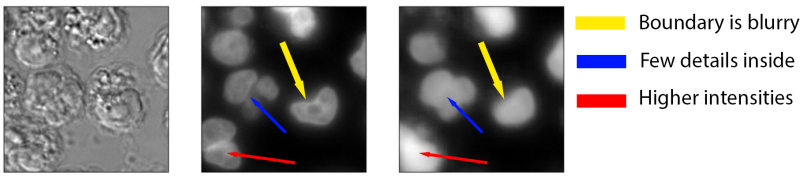


Figure 17: Problems in predictions

### 3.2.3 Postprocessing for nuclei segmentation

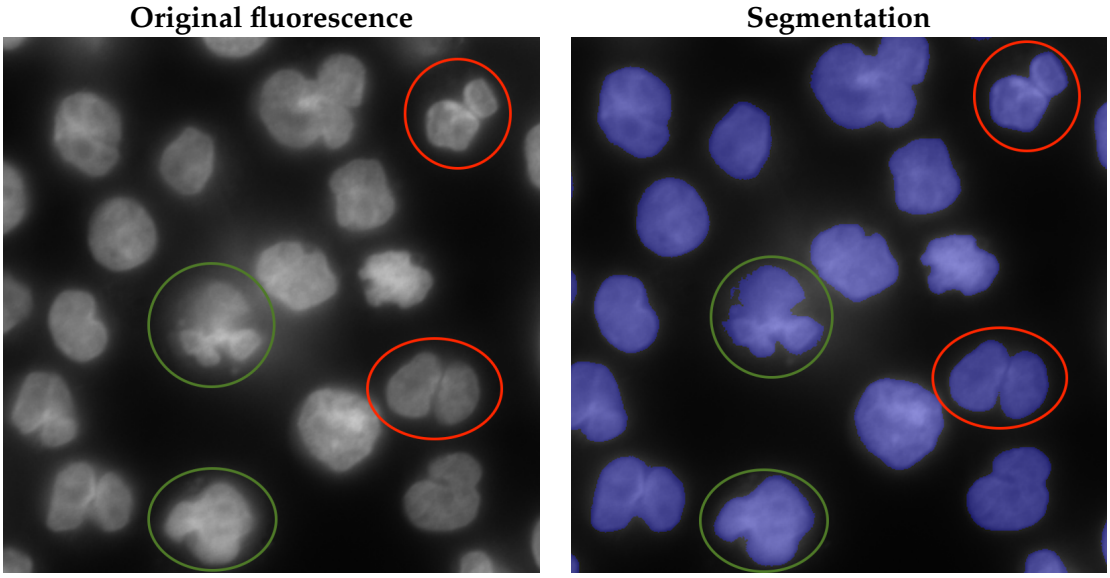


Figure 18: Closely located cells

Overall algorithm

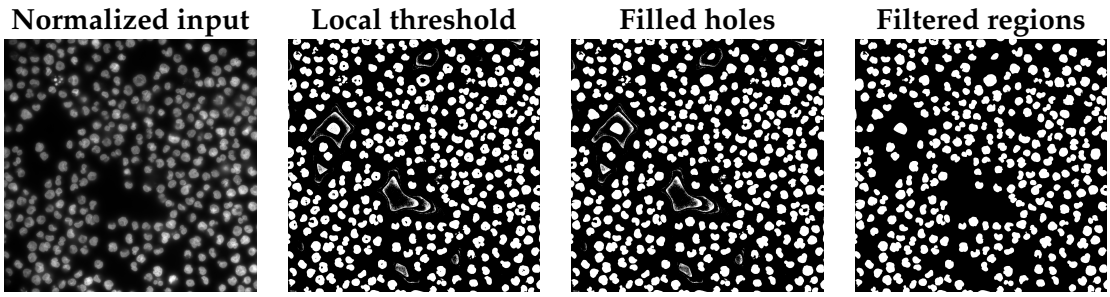


Figure 19: Fluorescence segmentation

### 3.2.4 Influence of scaling on predictions quality

Examples of predictions quality with different scales.

Table 2: Pearson correlation coefficients for downstream tasks for different scaling factors

| | 1.3 scale | 0.7 scale | Train (1.0 scale + augments) Predict (1.3 scale) | Train (1.3 scale) Predict (1.0 scale) | Train (1.3 scale) Predict (0.7 scale) |
|---|---|---|---|---|---|
| Number of nuclei | 0.987 | 0.995 | 0.975 | 0.971 | ? |
| Total intensity | 0.902 | .88 | 0.861 | 0.856 | ? |
| Mean intensity | 0.922 | 0.906 | 0.88 | 0.872 | ? |
| Area | 0.991 | 0.992 | 0.961 | 0.952 | ? |

## 3.3 Endoplasmic Reticulum

### 3.3.1 Preprocessing

**Algorithm 1** Fluorescence segmentation

1. Normalize image
2. Apply global *threshold_mean* to receive initial mask.
3. Zero out pixels outside the mask
4. Apply local thresholding.
5. Apply *fill_holes* transformation.
6. Morphological opening from OpenCV and Gaussian blur.
7. Run *findContours* from OpenCV in order to obtain separate regions and filter out too small regions.

Segmentation steps are also illustrated in Figure

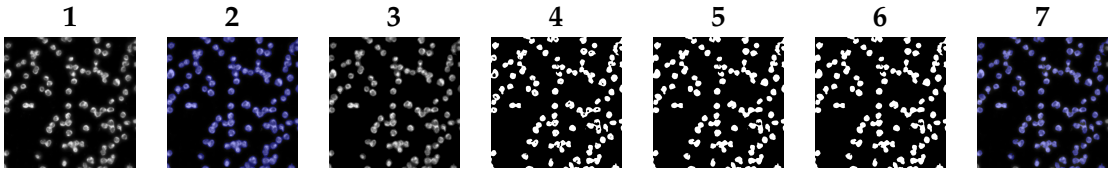


Figure 20: ER prediction

### 3.3.2 Training and predictions

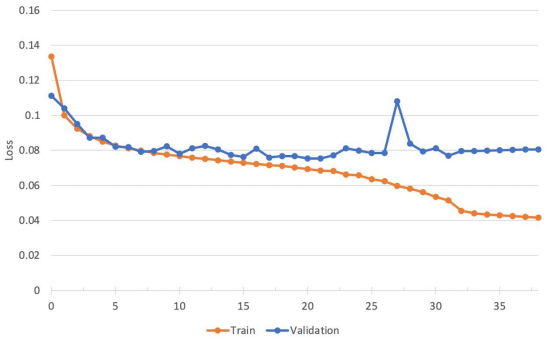


Figure 21: Overfit

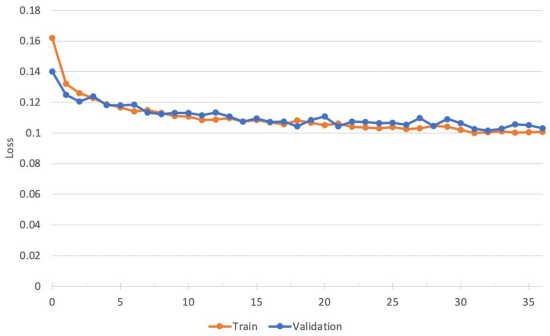


Figure 22: No overfit with augmentations

### 3.3.3 Combination of nuclei and actin predictions

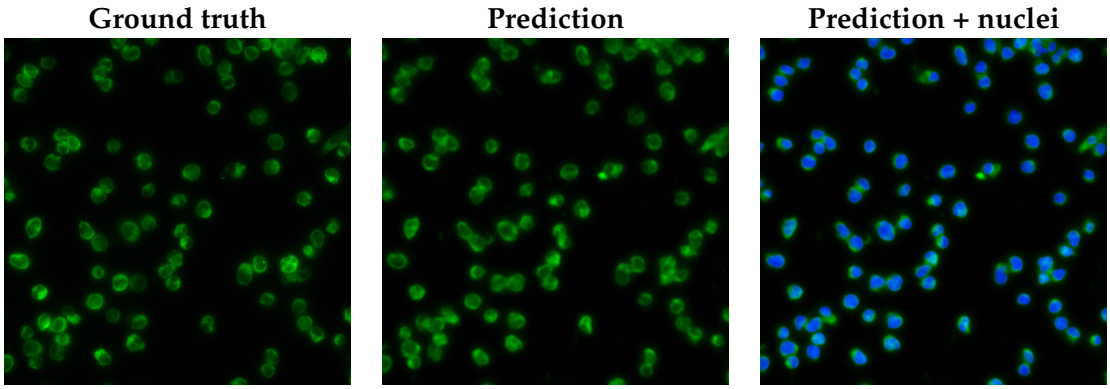


Figure 23: ER prediction

### 3.3.4 Generalizability across phenotypes

TODO train the model on one phenotype and predict on the other, compare predictions (visually?) postprocessing with metrics then? Add metrics

## 3.4 Golgi

### 3.4.1 Preprocessing

Enhancement

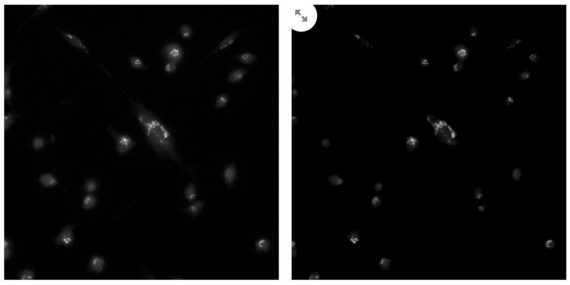

Figure 24: Golgi enhancement

#### 3.4.1.1 Background removal algorithms

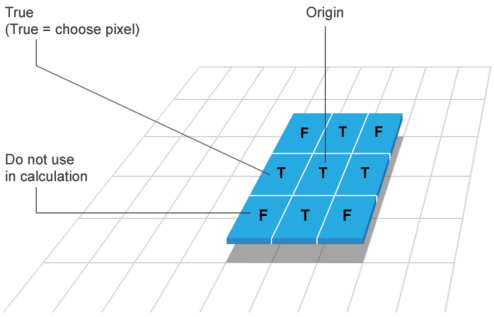


Figure 25: Structuring Element

Rolling ball algorithms

Rolling ball still leaves some noise

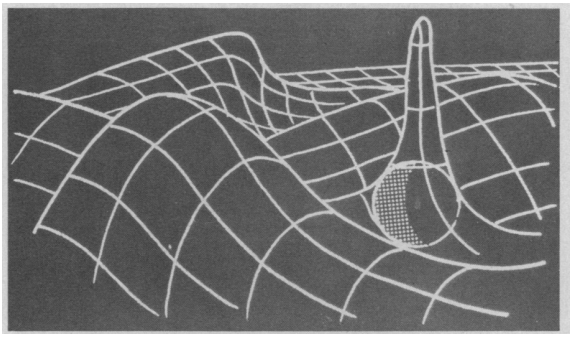

Figure 26: Rolling Ball

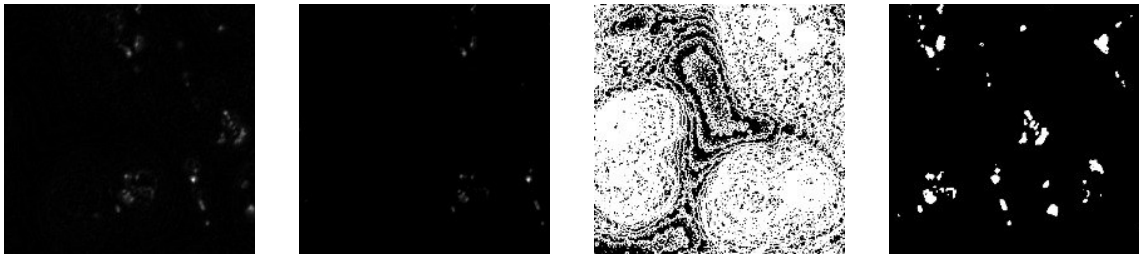

(a) (b) (c) (d)

Figure 27: (a) Vanilla pre-processing with automatic background removal algorithm only; (b) Additional clipping of lower intensities after vanilla pre-processing; (c) masked or subfigure (a); (d) mask of subfigure (b)

### 3.4.2 Training and predictions

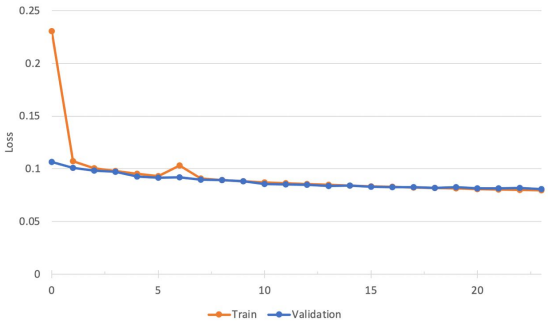


Figure 28: Straightforward training doesn't work

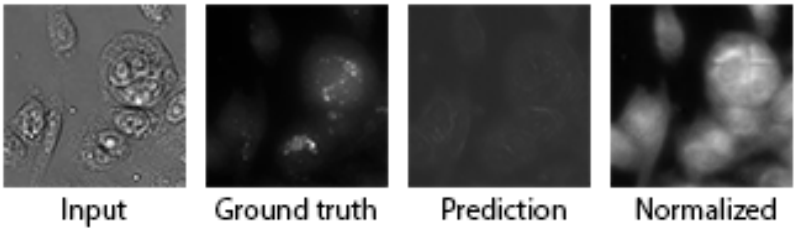


Figure 29: Training on original data

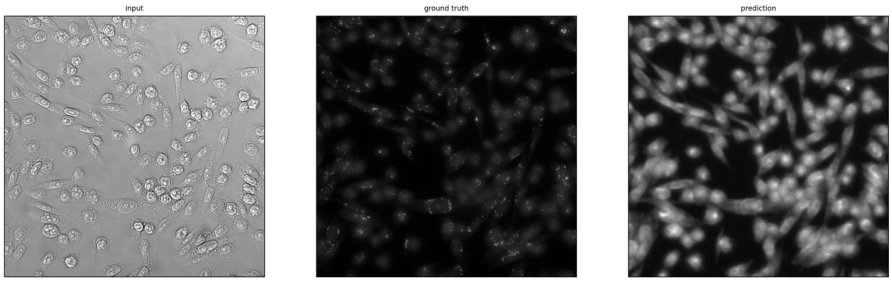


Figure 30: Full size predictions

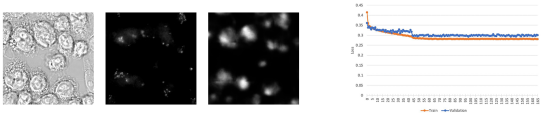

Figure 31: Training on the enhanced data

### 3.4.3 Alternative ways to improve predictions

#### 3.4.3.1 Asymmetrical losses

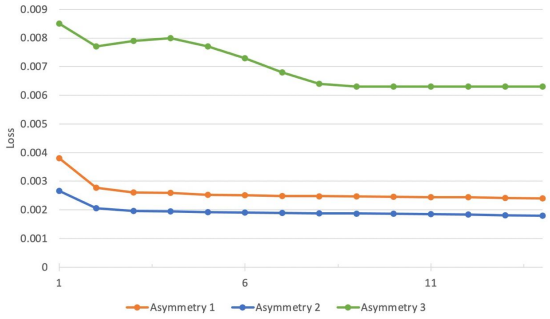


Figure 32: Asymmetrical training

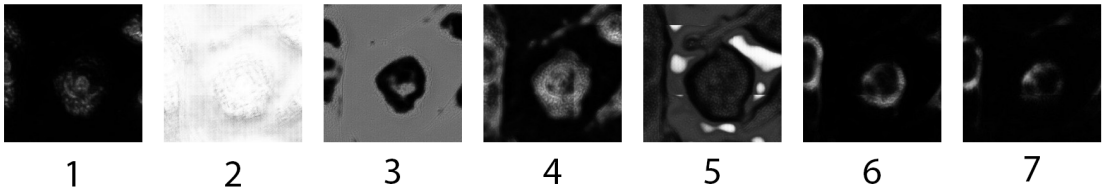


Figure 33: Asymmetrical training predictions

#### 3.4.3.2 Use of gradient in loss

#### 3.4.3.3 Noise reduction methods

## 3.5 GFP

### 3.5.1 Preprocessing

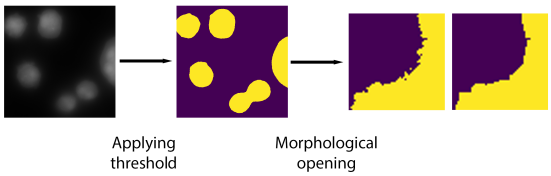


Figure 34: Converting GFP to a binary mask

### 3.5.2 Predictions

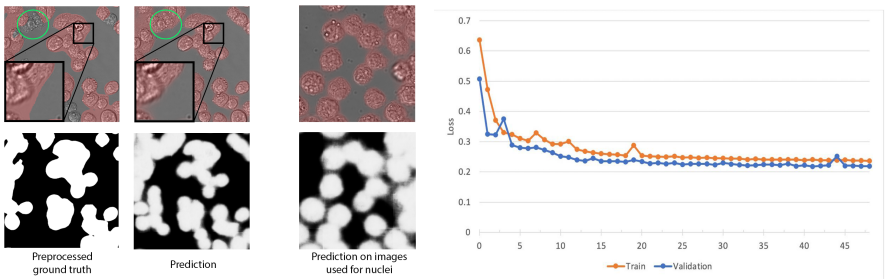


Figure 35: Training with BCE loss

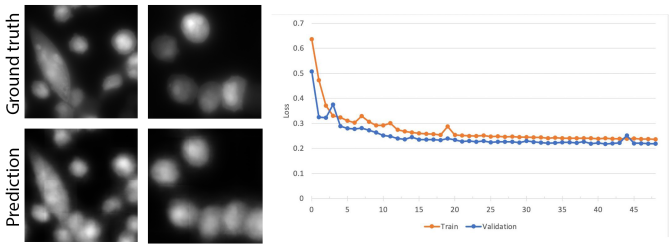


Figure 36: Training with Pearson correlation loss

Table 3: Correlation coefficients for downstream tasks

| Binary training | Pearson | Spearman |
|---|---|---|
| Number of ER | 0.67 | 0.64 |
| Area | 0.82 | 0.75 |
| **Continuos training** | **Pearson** | **Spearman** |
| Number of ER | 0.57 | 0.55 |
| Area | 0.26 | 0.64 |

### 3.5.3 Downstream metrics

TODO move to separate chapter?

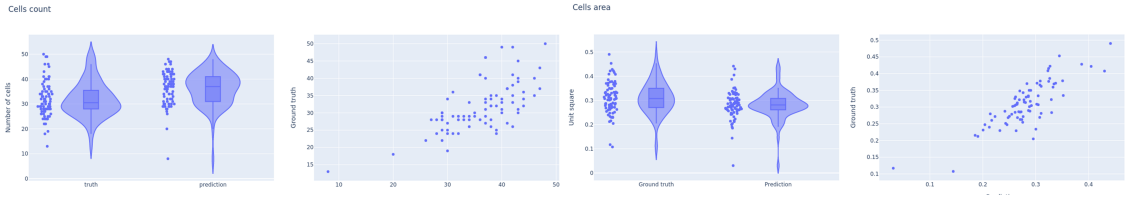


Figure 37: Downstream metrics

### 3.5.4 Combination of GFP, nuclei and ER

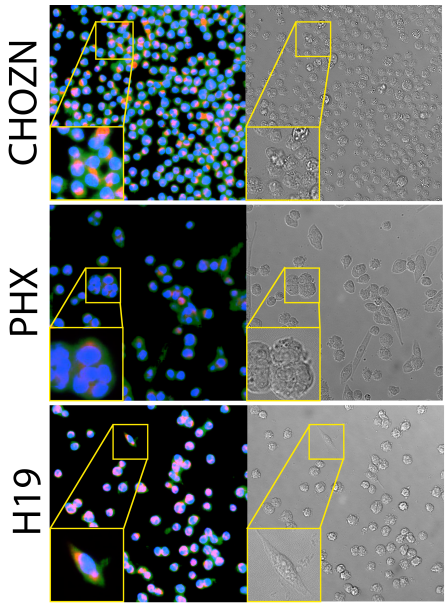


Figure 38: GFP, Nuclei and ER combined

## 3.6 Model evaluation

### 3.6.1 Metrics for downstream tasks

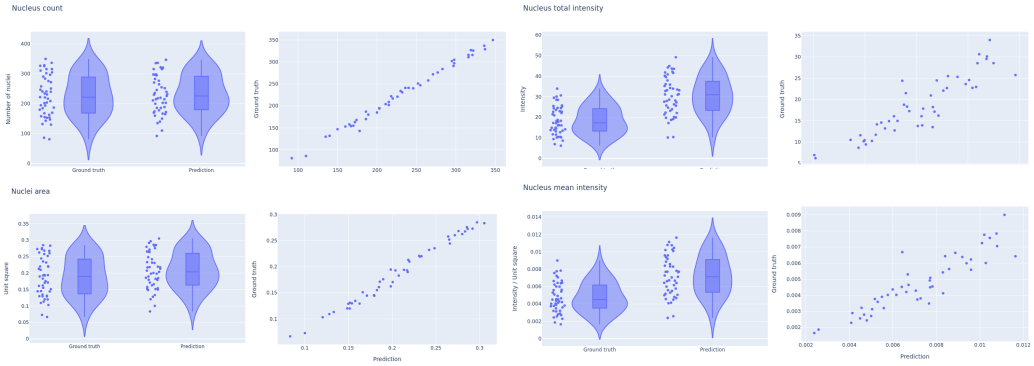


Figure 39: Metrics for downstream tasks on nuclei

Table 4: Correlation coefficients for downstream tasks on nuclei

| | Pearson | Spearman |
|---|---|---|
| Number of nuclei | 0.995 | 0.994 |
| Total intensity | 0.902 | .911 |
| Mean intensity | 0.907 | 0.904 |
| Area | 0.992 | 0.990 |

### 3.6.2 Influence of different loss functions on metrics for downstream tasks

# 4 Stability study

## 4.1 Stability study

### 4.1.1 Artificial corruptions

Description of artificial corruptions.

Table 5: Hyperparameterization for different artificial corruption severities

| Corruption \ Severity | -5 | -4 | -3 | -2 | -1 | 0 | 1 | 2 | 3 | 4 | 5 |
|---|---|---|---|---|---|---|---|---|---|---|---|
| Defocus blur (radius) | - | - | - | - | - | 0 | 0.5 | 1.0 | 1.5 | 2 | 3 |
| Contrast (gain) | 3.5 | 3.0 | 2.5 | 2.0 | 1.5 | 1 | 0.9 | 0.8 | 0.7 | 0.5 | 0.3 |
| Brightness (bias) | -150 | -135 | -120 | -90 | -50 | 0 | 50 | 90 | 120 | 135 | 150 |

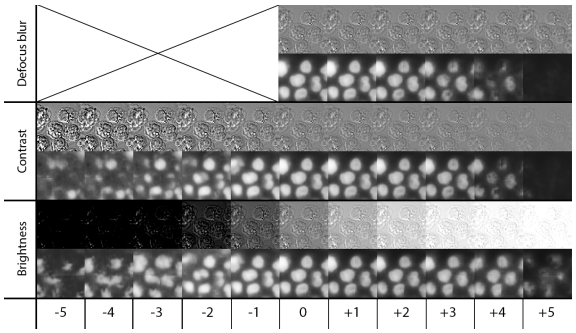


Figure 40: Influence of artificial corruptions on the predictions

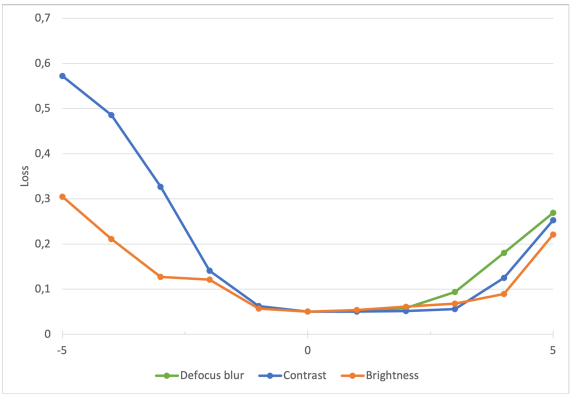


Figure 41: Change of Pearson correlation loss for artificial corruptions

### 4.1.2 Real corruptions

#### 4.1.2.1 Not fixed cells imaging as corrupted input

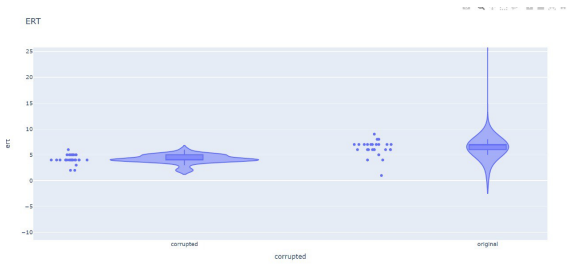


Figure 42: Online drift detection of not fixated cells

Scores of 0.91 however the threshold is 6, not corrupted data (fixed cells) mostly ert of 7 whereas corrupted data (not fixed cells) have an ert of 4. The threshold is therefore 6.

#### 4.1.2.2 Real-world examples of corruptions

### 4.1.3 Influence of corruptions on metrics for downstream tasks

Calculate how metrics worsen when the evaluation stays the same, but the input is corrupted.

### 4.1.4 Improving predictions with additional corruption augmentations

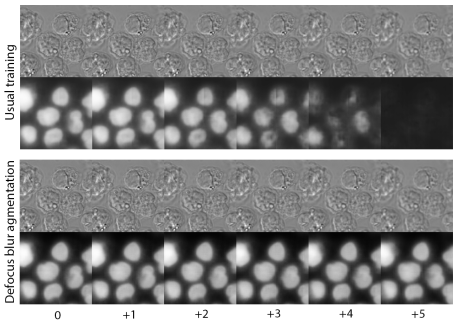


Figure 43: Using corruptions as augmentations improves predictions

## 4.2 UNET embeddings study

### 4.2.1 Application of various dimentionality reduction methods

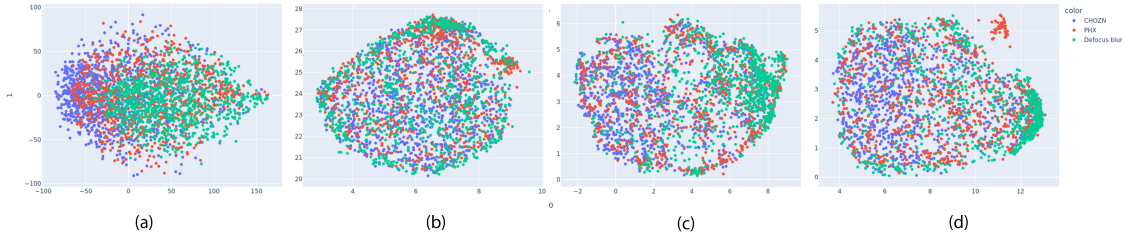


Figure 44: (a) PCA, (b) UMAP, (c) combination of PCA and UMAP with 10 and (d) 50 components

### 4.2.2 Autoencoder embeddings as an alternative

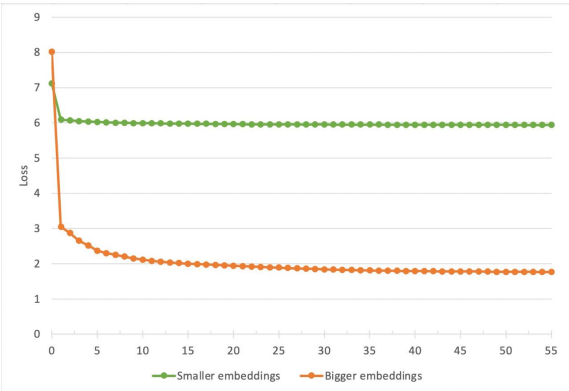


Figure 45: Autoencoders training convergence

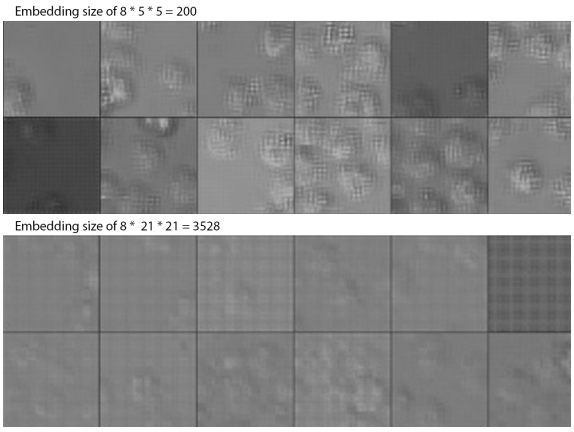


Figure 46: Samples drawn from the trained autoencoder

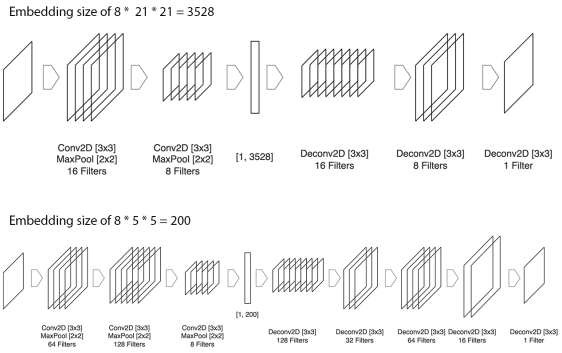


Figure 47: Architectures of two autoencoders

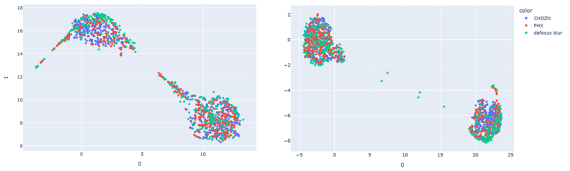

Figure 48: Autoencoder embeddings after applying PCA with 10 components and UMAP afterwards. Earlier epoch VS later epoch

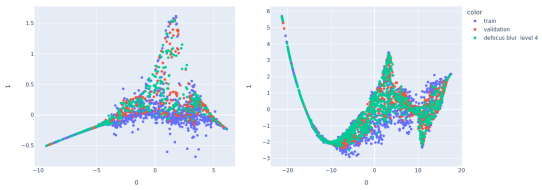


Figure 49: PacMAP does not provide information on the coruption

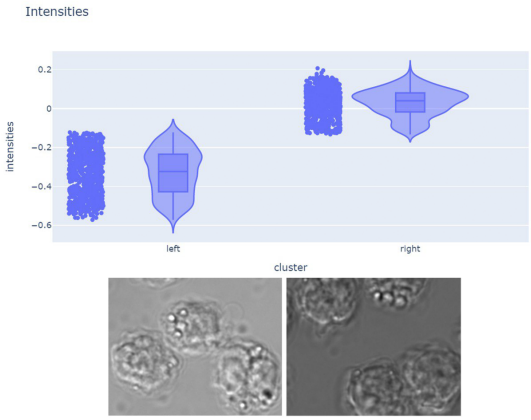


Figure 50: What do two UMAP clusters represent

### 4.2.3 Clustering of PacMAP embeddings

#### 4.2.3.1 Clustering on UNet embeddings

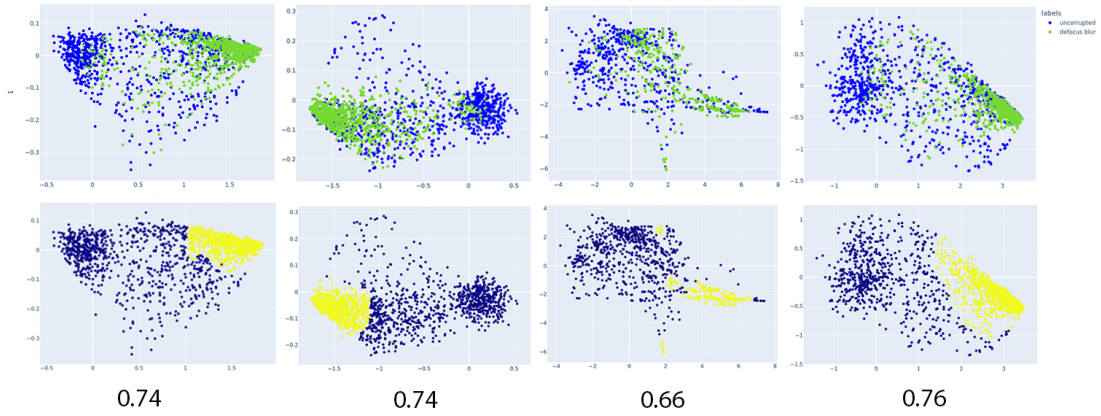


Figure 51: Clustering of UNet embeddings after PacMAP

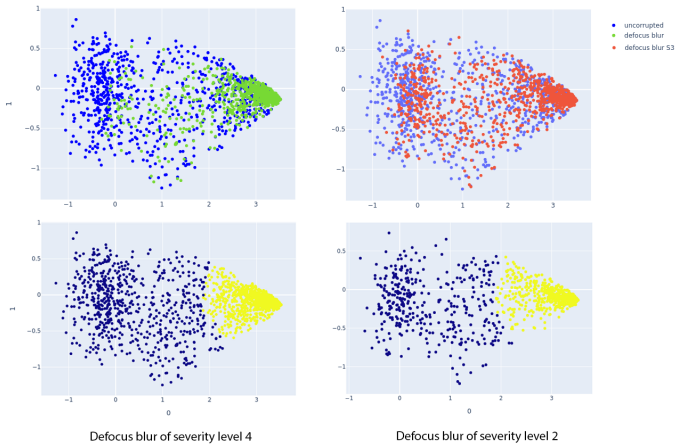


Figure 52: Clustering of UNet embeddings after PacMAP for different severities levels

TABLE with F1-score: 0.76 VS 0.64

## 4.3 Drift detection

### 4.3.1 A need to detect drift

### 4.3.2 Maximum mean discrepancy for drift detection

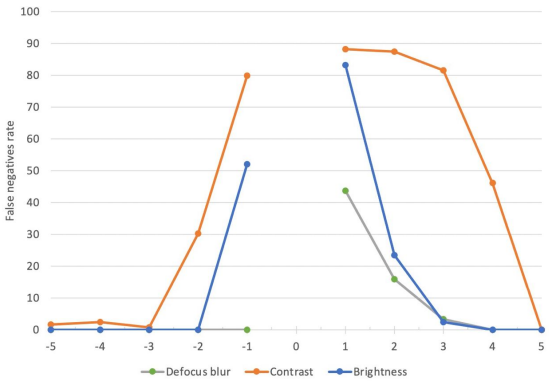


Figure 53: False negatives rate for drift detection on artificial corruptions

### 4.3.3 Online version of MMD algorithm

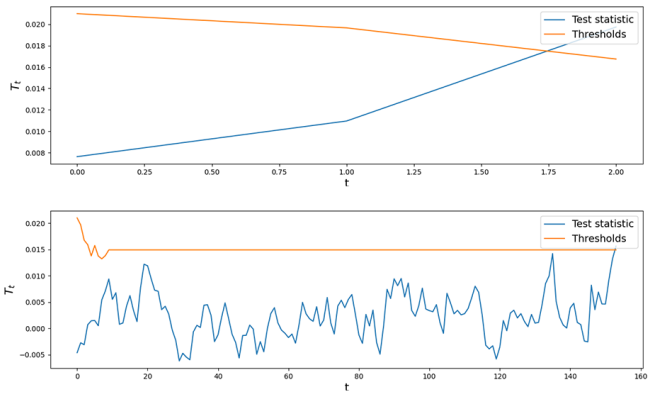


Figure 54: Expected runtime (ERT) for corrupted and in-distribution data

Table 6: Test window size influence on separability

| W | 2 | 5 | 10 | 15 | 20 |
|---|---|---|---|---|---|
| Auc-Roc | 0.85 | 0.92 | 0.98 | 0.90 | 0.88 |

Table 7: ERT influence on separability

| W | 32 | 64 | 128 | 256 |
|---|---|---|---|---|
| Auc-Roc | 0.90 | 0.95 | 0.98 | 0.98 |

Table 8: Severity of corruptions on separability

| W | Level 2 | Level 3 | Level 4 |
|---|---|---|---|
| Auc-Roc | 0.84 | 0.92 | 0.98 |

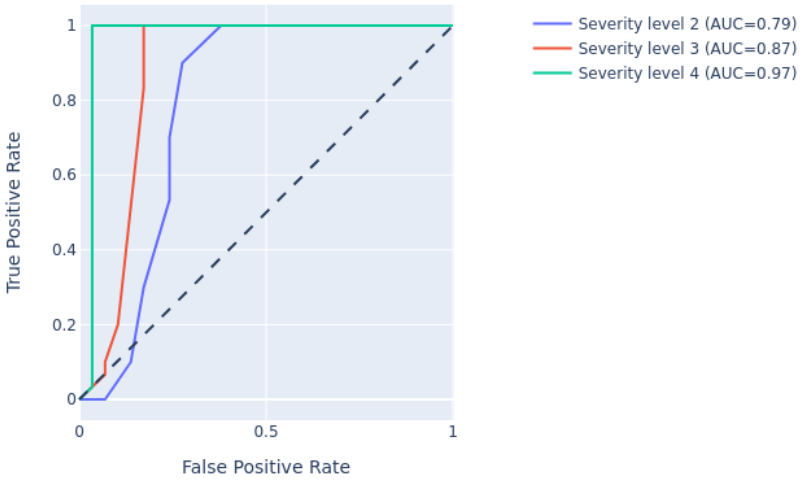


Figure 55: AUC ROC scores for various defocus corruptions severities

# 5 Software Tools

## 5.1 Foundry. Palantir

## 5.2 AWS

## 5.3 Streamlit

# 6 Future research

" One limitation of our current work is that it is based on fixed cells that does not allow longitudinal imaging. This can be overcome by using fluorescent reporter cell lines or live cell dyes to provide the fluorescence ground truth (10) and enable dynamic observation. Another limitation of the DL framework we used here is that it cannot be generalized to different types of cells. Techniques based on transfer learning (https://doi.org/10.1038/s41551-019-0362-y, https://downloads.spj.sciencemag.org/bmef/2020/9647163.pdf) and domain adaptation (38) will be investigated in our future work to overcome this limitation." TODO rephrase https://www.science.org/doi/10.1126/sciadv.abe0431

# 7 Summary

# List of Figures

## List of Tables